Structural Anomalies of Rb and Br Ionic Nanosolutions in Hydrophobic Slit-Shaped Solid Space as Revealed by the EXAFS Technique

Takahiro Ohkubo,[†] Yoshiyuki Hattori,[‡] Hirofumi Kanoh,[†,§] Takehisa Konishi,[†,§] Takashi Fujikawa,[†,§] and Katsumi Kaneko*[,†,§]

Department of Chemistry, Faculty of Science, Chiba University, 1-33 Yayoi, Inage, Chiba 263-8522, Japan, Institute of Research and Innovation, 1201 Takada, Kashiwa, Chiba 277-0861, Japan, and Center for Frontier Electronics and Photonics, Chiba University, 1-33 Yayoi, Inage, Chiba 263-8522, Japan

Received: February 12, 2003; In Final Form: September 17, 2003

The hydration structure of RbBr electrolytic solutions confined in slit-shaped nanospaces of carbon was determined with the extended X-ray absorption fine structure (EXAFS) technique and related analysis. The nitrogen adsorption isotherms at 77 K were measured to evaluate the porosity of RbBr-deposited carbon samples. The EXAFS results indicate that the electrolytic solution confined in hydrophobic nanospaces has a restricted hydration structure depending on the average pore width of the nanospaces. Also the asymmetric-field effect of slit-pore geometry on the formation of unique hydration structures of ions in nanospaces was unveiled with the analysis of EXAFS spectra. A marked decrease of the hydration number around a Rb ion was observed in slit-shaped nanospaces, indicating the compressed hydration structure around a Rb ion restricted in slit-shaped nanospaces. The distorted hydration structure around a Br ion in the slit-shaped pore of 0.7 nm was formed to increase the hydration number, though partially dehydrated structure can be formed in a 1.1-nm pore. The cluster-mediated ordered structure of water molecules can play an important role in forming a dehydrated structure around a Br ion confined in the 1.1-nm pore.

1. Introduction

The confinement effect in solid nanospaces has gathered much attention, because nanoconfinement holds intensive possibilities for new science and the fundamental understanding can be helpful in developing better technologies relating to gas storage, gas separation, purification, and electronic devices.[1,2] However, the study of nanoconfinement has just started and the nature of confinement in nanoscale space is not sufficiently understood. We have been challenged to elucidate the adsorption phenomena in solid nanospaces from the above viewpoint, reporting that the molecules adsorbed in hydrophobic nanospaces tend to form a highly ordered structure depending on the pore width and properties of adsorbate molecules.[3−6] For example, water and alcohol molecules adsorbed in the slit-shaped carbon micropores form a highly ordered structure even at 303 K as revealed by the in situ X-ray diffraction (XRD) technique.[7−10] Also CCl_4,[11] NO,[12] and Xe[13] form a highly condense structure in the micropores even at 303 K, as if these molecules were compressed. This effect is named the pseudocompression effect. The phase transition in solid nanospaces is also characteristic, which is significantly different from that of the bulk phase.[14−17]

The chemistry of ionic solutions has been devoted to understanding electrochemistry, analytical chemistry, biochemistry, catalysis, and synthetic chemistry. The classical hydration model, such as the Frank−Wen model,[18] is indeed helpful in understanding the properties of electrolytic solution. However, we wonder if such a model can be applied to nanoscale phenomena and structures. Hribar et al. showed that the hydrated structures of water strongly depend on the charge density of a central ion using Monte Carlo simulation: an ion having high charge densities can break hydrogen bonds to hydrate with adjacent water molecules.[19] Although hydrated structures and hydrogen bonds around an ion have been studied independently, a wider scope study on nanorange structures around an ion including hydration structures and hydrogen bonds should be carried out. Also new research efforts for ionic solution chemistry are aimed at how to determine precisely the hydrated structure under special conditions such a supercritical condition.[20,21] Fulton et al., for instance, reported anomalous hydration structures around a Rb ion in supercritical water;[22] they reported that the coordination distance between a cation and an oxygen atom of water is reduced by 0.01 nm and the coordination number decreases by 40% compared with that of normal RbBr aqueous solution under ambient conditions. This study indicates that even the first hydration shell can vary with the local environment. Consequently, the exposure of electrolytic solution to a special condition can provide a new direction in solution chemistry. We applied well-characterized hydrophobic nanospaces to study the hydration structures around an ion.

Iiyama et al. showed that the molecular assembly of water confined in the slit-shaped nanospace of ACF is close to solid even at 303 K and the structure is more ordered in narrower spaces revealed by in situ X-ray diffraction.[7,8] They also showed the dependence of the cluster growth of water molecules with pore width of ACF by in situ small-angle X-ray scattering.[23] Kimura et al. showed the change of heat of water adsorption with the pore widths of 0.7 to 1.2 nm for ACF.[24] Therefore, the ordered structure and cluster formation of water molecules in the carbon nanospaces of ACFs is sensitive to the pore width. Consequently, the structure of ionic solution confined in

* Author to whom correspondence should be addressed. Phone: 81-43-290-2779. Fax: 81-43-290-2788. E-mail: kaneko@pchem2.s.chiba-u.ac.jp.
[†] Department of Chemistry, Faculty of Science, Chiba University.
[‡] Institute of Research and Innovation.
[§] Center for Frontier Electronics and Photonics, Chiba University.

10.1021/jp0343685 CCC: $25.00 © 2003 American Chemical Society
Published on Web 11/15/2003

nanospaces should depend on the pore width. Then we examined the pore-width dependence of the restricted hydration structure using two kinds of ACF having different pore widths.

An extended X-ray absorption fine structure (EXAFS) technique is quite effective in determining the local structure around a target atom. Then we applied EXAFS to study the nanoscale RbBr solution confined in the slit-shaped hydrophobic nanospace of activated carbon fiber (ACF), showing a hydration anomaly in the preceding communication.[25] However, even the EXAFS technique has a serious limitation in analysis due to confinement of target atoms in the nanospace. The cumulant expansion analysis of the EXAFS spectrum can provide a more exact local structure around the target atom. This article describes the nanospace size dependence of the hydration anomaly around Rb and Br ions in the hydrophobic nanospaces of ACF, which was evidenced with the EXAFS using the cumulant expansion analysis.

2. Experimental Section

2.1. Sample Preparation. Two kinds of pitch-based ACF (P5 and P20; AD′ALL Co. Ltd.) were used, because authors published much evidence that ACF has considerably uniform slit-shaped hydrophobic nanospaces.[26−30] Also the preceding studies showed that pitch-based ACF has the least number of surface functional groups. Hence pitch-based ACF was used to focus the discussion on the confinement effect of hydrated ions. We used RbBr as an electrolyte, because these are suitable for the EXAFS measurements. The electrolytic aqueous solutions of 0.1 and 1 mol/dm^3 were introduced into the slit-shaped micropores of ACFs, which were dried by evacuation at 0.1 mPa and 383 K for 2 h. After the deposition of RbBr, water vapor was adsorbed to provide the corresponding solution only in the carbon nanospaces at the relative pressure over 0.9; the obtained solution is called the nanosolution[25,31] (NSN) in this article. We denote, for instance, the NSN made by RbBr of 1 mol/dm^3 aqueous solution on P20 as P20-NSN-1M.

2.2. Porosity of ACFs Deposited by RbBr. The high-resolution N_2 adsorption isotherms of ACFs and RbBr-deposited ACFs at 77 K were measured and the porosity for each sample was determined by subtracting the pore effect (SPE) method for the high-resolution α_s plot.[32,33] Also the weight ratio of deposited RbBr, the volume filling of RbBr in micropores, and the molar concentration of RbBr in micropores are calculated by using the pore parameter, except for the weight ratio of RbBr, which is obtained from weight changes between before and after the deposition of RbBr on ACFs. Especially, the volume filling of RbBr in ACF, θ_{RbBr}, can be described by the pore volume of RbBr-deposited ACFs per gram, V_s, the pore volume of ACF per gram, V_{ACF}, and the weight ratio of RbBr, γ:

$$\theta_{RbBr} = 1 - \frac{V_s}{V_{ACF}} = 1 - \lambda(1 + \gamma) \qquad (1)$$

where

$$\lambda = \frac{V_s'}{V_{ACF}} \qquad (2)$$

Here, V_s' is the pore volume of RbBr-deposited ACF per gram, which is obtained experimentally.

2.3. EXAFS Measurements and Analytical Methods. These samples were installed in an EXAFS glass cell with windows of Lumirror film (350 μm: Toray Ind. Inc.). The EXAFS measurements were performed on both Rb and Br K-edges for the NSNs at the National Laboratory for High Energy Accelerator Research Organization (KEK) in Tsukuba. The EXAFS spectra of the corresponding solutions were measured for comparison. The radial structure functions (RSFs) for Rb and Br ions were obtained from the EXAFS.

The structure determination was carried out by curve fitting of the reverse Fourier transformed function of the definite shell in each RSF with the formula of EXAFS spectra, $\chi(k)$, including the structural parameters around a central atom:[34]

$$\chi(k) = N|F(k)|e^{-2\sigma^2k^2}e^{-2r/\lambda(k)}\frac{\sin(2kr + \phi(k))}{kr^2} \qquad (3)$$

Here, k is the wavenumber of a photoelectron, N is the coordination number around a central atom, $F(k)$ is the back-scattering amplitude of a central atom, σ is the Debye−Waller (DW) factor related to the disordering of the neighboring shell, $\lambda(k)$ is the mean free path length of a photoelectron, $\phi(k)$ is the total phase shift by the photoelectron, and r is the distance between a central atom and the neighboring shell. The calculated parameters of $F(k)$, $\lambda(k)$, and $\phi(k)$ obtained by FEFF procedure[35] were used in the curve fitting.

3. Results and Discussion

3.1. Determination of Porosity for ACF Deposited by RbBr. The N_2 adsorption isotherms on ACFs and RbBr-deposited ACFs were of type I, as shown in Figure 1. These data were used for the determination of the micropore structures with the SPE method for the high-resolution α_s plot. The micropore volume, total surface area, external surface area, and the average pore width are collected in Table 1. Also the weight ratio of deposited RbBr, the volume filling of RbBr in micropores, and the molar concentration of RbBr in micropores are calculated by using the pore parameter except for the weight ratio of RbBr, which is obtained from weight changes between before and after the deposition of RbBr on ACFs. These parameters indicate that the weight of deposition on P5 of $w = 0.7$ nm is small compared with that of P20 ($w = 1.1$ nm). Diameters of the hydrated ions of a six-coordination structure are calculated to be approximately 0.86 and 0.95 nm for a Rb and a Br ion, respectively. Accordingly, the fully hydrated ions are difficult to enter in the 0.7 nm slit width space and thereby the deposition amount of RbBr in micropores of P5 is smaller than that of P20. The volume filling of RbBr in P5, on the other hand, is larger than that of P20. Therefore, the micropore spaces of P5 must be more effectively filled with RbBr than those of P20 although the deposited RbBr can inhibit the further adsorption of nitrogen to increase the volume filling of RbBr in nanospaces effectively. The deposition results on P20 show that the higher the concentration of aqueous solution, the more ions are in the micropores because of the greater gradient of concentration. In the case of the dilute solution, the ions tend to be adsorbed near the entrance of the micropores, blocking further adsorption of ions in deeper pore sites. Thus the filling by RbBr molecules is markedly affected by both the concentration of aqueous solutions and the average micropore widths.

3.2. Restricted Hydration Structure of Confined Nanosolutions in 1.1 nm Slit Space. Figure 2 shows the RSFs of NSNs in P20 around a Rb ion. RSFs of bulk 1 mol/dm^3 RbBr aqueous solutions are shown for comparison. The RSFs of NSNs are close to that of bulk solution, although they are slightly noisy at higher coordination shells. The highest peak around 0.20 nm is assigned to the Rb−O coordination of the nearest hydration

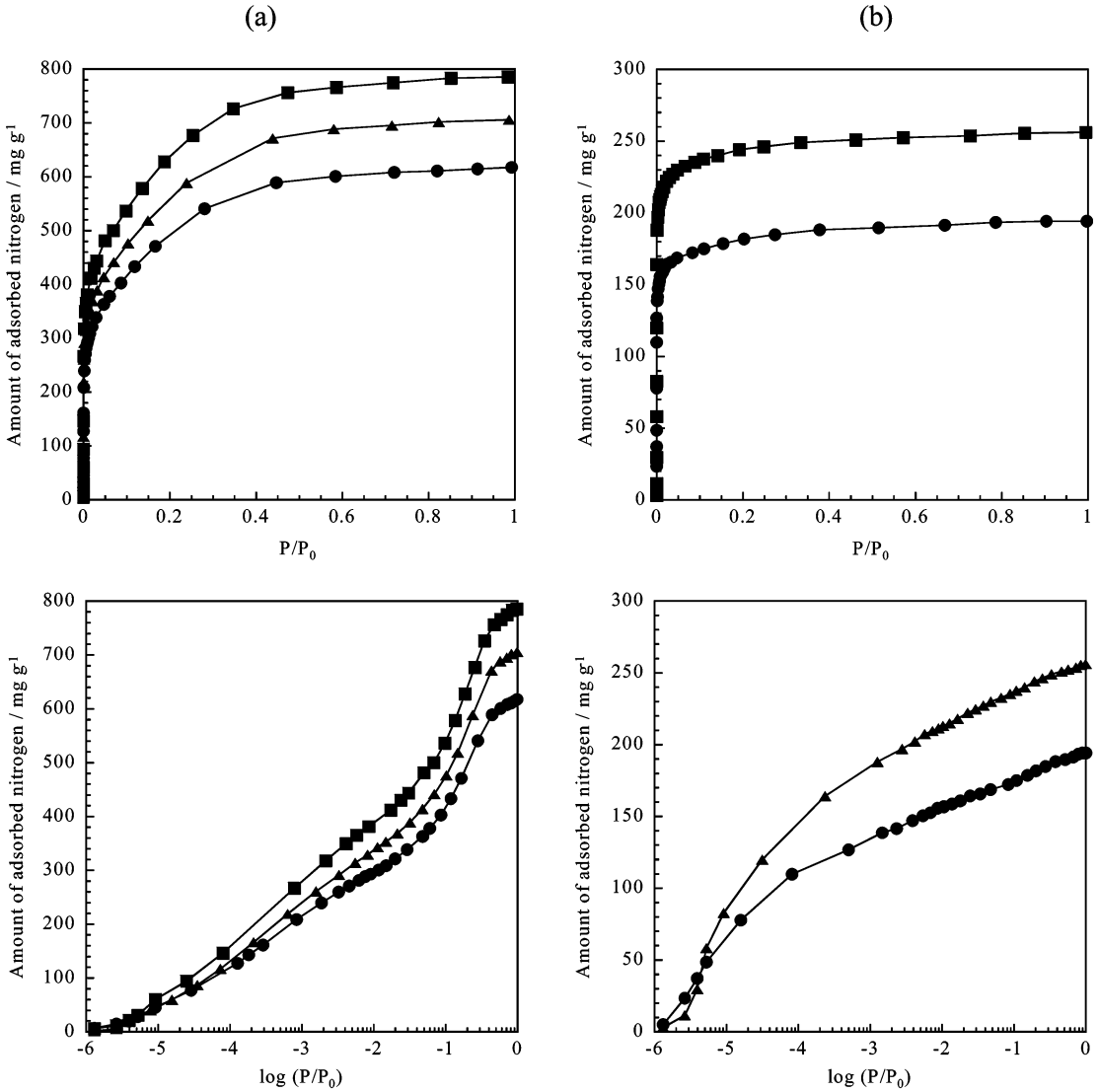

Figure 1. Adsorption isotherms of nitrogen on RbBr-deposited P20 (a) and P5 (b) at 77 K: (●) deposited by 1 mol/dm^3 RbBr solution; (▲) deposited by 0.1 mol/dm^3 RbBr solution; (■) original ACFs. The horizontal axis of each bottom figure is expressed by the logarithm of relative pressure for the horizontal axis.

TABLE 1: Pore Structural and Electrolyte Parameters of ACFs and RbBr-Deposited ACFs[a]

sample	a_α/ m^2 g^{-1}	a_{ext}/ m^2 g^{-1}	W_0/ mL g^{-1}	w/ nm	γ/ wt %	θ_{RbBr}/ %
P5-NSN-1M	680	9	0.23	0.69	3.2	19
P5	930	11	0.30	0.65	0	0
P20-NSN-1M	1290	33	0.72	1.1	21	5.3
P20-NSN-0.1M	1580	34	0.83	1.1	5.3	5.0
P20	1730	40	0.92	1.1	0	0

[a] The parameters are total surface area a_α, external surface area a_{ext}, micropore volume W_0, average pore width w, weight ratio of deposited RbBr γ, and volume filling of RbBr in micropore θ_{RbBr}.

shell. Figure 3 shows the Br-centered RSFs of NSNs and the bulk aqueous solution of 1 mol/dm^3. All samples have a main peak around 0.25 nm, which is assigned to the hydration structure (Br−O). Only the 1st hydration shell around a Rb and a Br ion can be analyzed because no explicit peaks from 2nd and 3rd coordination shells around a Rb and a Br ion can be obtained by EXAFS measurements. In addition, as the coordination distance of Figures 2 and 3 cannot be used for determination of the local structures, we must correct the data by curve fitting before discussion. Therefore we determine the coordination distance and other structural parameters of only the 1st hydration shell by the reverse Fourier transformation and fitting treatment for each sample.

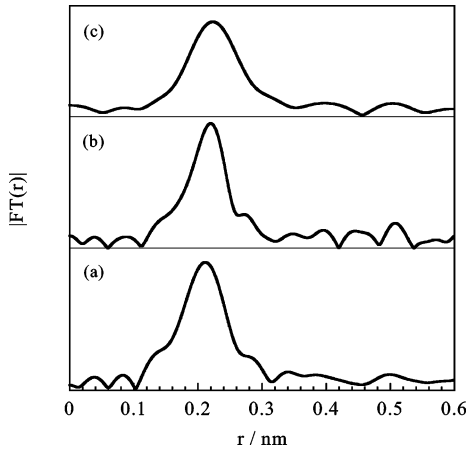

Figure 2. Radial structure functions around a Rb ion for NSNs on P20: (a) P20-NSN-1M; (b) P20-NSN-0.1M; (c) bulk aqueous solution of 1 mol/dm^3 RbBr.

The parameters obtained by curve fitting are summarized in Table 2. Explicit features of the structures of NSNs in P20 are

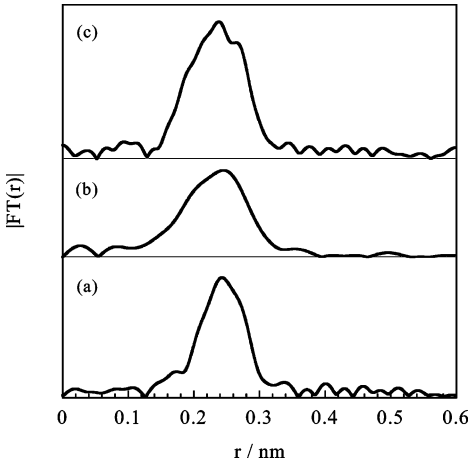

Figure 3. Radial structure functions around a Br ion for NSNs on P20: (a) P20-NSN-1M; (b) P20-NSN-0.1M; (c) bulk aqueous solution of 1 mol/dm^3 RbBr.

shown as follows. The average Rb−O distance of the NSNs in P20 is clearly smaller than that of the bulk RbBr aqueous solution obtained in this work. The literature value for the Rb−O distance is in the range of 0.287−0.312 nm,[36−40] although these literature values depend on the experimental techniques and analytical methods. The coordination number of hydrated water molecules around a Rb ion in the nanospace is remarkably less than that in the bulk aqueous solution. The average DW factor around a Rb ion for NSNs is smaller than that in the bulk aqueous solution. Here, the smaller DW factor means the presence of more ordered structures. Therefore, the hydration structure of NSN around a Rb ion should be more ordered compared with that of the bulk aqueous solution. In the case of hydration structures around a Br ion, the analyzed coordination distance in micropores is close to the Br−O distance in bulk aqueous solution, which is in the literature value range of 0.29−0.34 nm.[36,41−45] The hydration number and DW factor around a Br ion of NSNs in P20 are much smaller than that of the bulk solution. Accordingly, the hydration structure around a Br ion is remarkably restricted to form a smaller hydration structure of more ordering as well as that around a Rb ion. On the other hand, the structural changes of NSNs in P5 are different from those in P20, as shown in the next section.

We should discuss the reliability of the curve fitting using the *R*-factor, which is defined as:

$$R(\%) = \frac{\sqrt{\sum\{\chi^{\mathrm{data}}(k) - \chi^{\mathrm{fit}}(k)\}^2}}{\sqrt{\sum\{\chi^{\mathrm{data}}(k)\}^2}} \times 100 \qquad (4)$$

Here, $\chi^{\mathrm{data}}(k)$ and $\chi^{\mathrm{fit}}(k)$ are the EXAFS functions of the experimental data and the fitting function, respectively. As long as the signal-to-noise (S/N) ratio of the data is not so small, the *R* of an adequate fitting can be expected to be not more than a few percent.[46] Table 2 also shows the *R*-factor for each sample. The *R*-factor for the ionic solution around a Br ion is larger than that around a Rb ion. All curve-fitting procedures in this study were carried out for six-coordinated hydration structures at definite distances around both a cation and an anion as an ideal model. Therefore, the nonideal effect or the change of the coordination structures around a Br ion must be more predominant than those around a Rb ion. These effects must be taken into account in a further analysis.

3.3. Pore-Width Dependence of Restricted Hydration Structure of Nanosolutions. Figure 4 shows RSFs of NSN in P5 around a Rb ion. The peak of the first hydration shell for P5-NSN-1M is relatively distinct compared with that of bulk aqueous solution, indicating the highly ordered structure of the first hydration shell for this NSN. RSFs around a Br ion for P5-NSN-1M and a bulk aqueous solution of 1 mol/dm^3 are shown in Figure 5. Both RSFs are similar, which is different from the RSFs around a Rb ion. These RSFs were analyzed with the curve fitting procedure to assign precisely the main peak.

TABLE 2: Structural Parameters Obtained by a Least-Squares Fit of Fourier-Filtered EXAFS Spectra[a]

sample	$r_{\mathrm{Rb-O}}$/ nm	$N_{\mathrm{Rb-O}}$	$\sigma^2_{\mathrm{Rb-O}}$/ 10^{-5} nm^2	$R_{\mathrm{Rb-O}}$/ %
P20-NSN-1M	0.275(±0.001)	3.5(±0.1)	22.7(±0.6)	8.9
P20-NSN-0.1M	0.280(±0.001)	2.5(±0.1)	19.3(±0.5)	8.1
P5-NSN-1M	0.271(±0.001)	4.7(±0.2)	23.5(±0.6)	9.0
RbBr soln (1 M)	0.295(±0.001)	6.0[b]	26.2(±0.6)	10.6
sample	$r_{\mathrm{Br-O}}$/ nm	$N_{\mathrm{Br-O}}$	$\sigma^2_{\mathrm{Br-O}}$/ 10^{-5} nm^2	$R_{\mathrm{Br-O}}$/ %
P20-NSN-1M	0.324(±0.001)	4.0(±0.1)	16.2(±0.4)	5.7
P20-NSN-0.1M	0.315(±0.001)	3.5(±0.4)	15.1(±1.9)	27.3
P5-NSN-1M	0.317(±0.001)	9.2(±0.6)	30.6(±1.6)	16.0
RbBr soln (1 M)	0.319(±0.001)	6.0[b]	18.4(±0.2)	7.9

[a] The parameters are interatomic distance *r*, relative coordination number *N*, Debye−Waller factor σ, and *R*-factor *R*. The first and second elements in the subscripts denote the central and scattering atoms, respectively. [b] Fixed parameter.

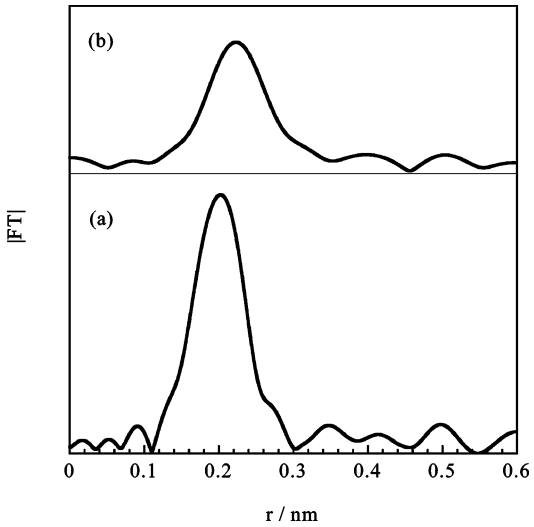

Figure 4. Radial structure functions around a Rb ion for NSNs on P5: (a) P5-NSN-1M; (b) bulk aqueous solution of 1 mol/dm^3 RbBr.

The parameters of NSN in P5 from curve fitting are summarized in Table 2. The Rb−O distance of the NSNs in P5 is much smaller than that of NSNs in P20. However, the coordination number of water molecules around a Rb ion of P5-NSN-1M is considerably larger than that of NSNs in P20. The short Rb−O distance and large coordination number indicate the highly compressed state around a Rb ion in micropores of P5. The smaller DW factor than that of bulk aqueous solution also reflects a more ordered structure due to the nanoconfinement effects of hydration structure around a Rb ion. On the other hand, the coordination distance of P5-NSN-1M around a Br ion is the same as that of the bulk solution of RbBr whereas the coordination number of this sample is quite large. Thus the local structure anomalies around a Rb and a Br ion in the 0.7-nm pores are different from those in the 1.1-nm pores.

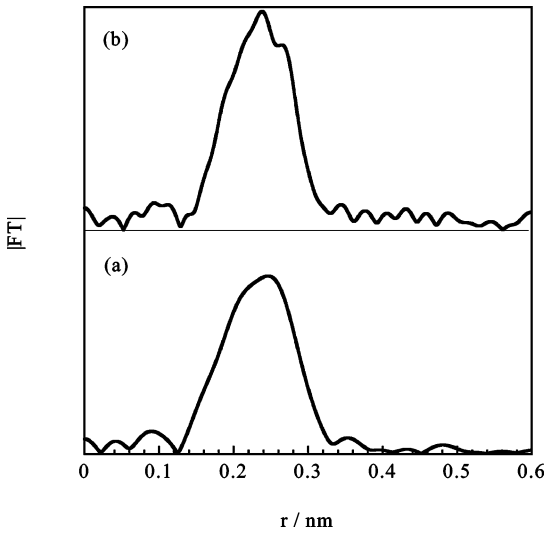

Figure 5. Radial structure functions around a Br ion for NSNs on P5: (a) P5-NSN-1M; (b) bulk aqueous solution of 1 mol/dm^3 RbBr.

The observed hydration structure anomalies should stem from the pseudocompression effect of hydrophobic micropores. The pseudocompression effect arises from the presence of the enhanced molecule−pore wall interaction potential; molecules tend to be adsorbed in the micropores as much as possible, when the enhanced potential is sufficiently larger than thermal energy at the adsorption temperature. Smaller pores can induce a strong pseudocompression effect. A water molecule does not interact strongly with the carbon micropore, while the cluster of the pentamer size of water molecules loses the ionic nature, giving rise to an intensive interaction even with the hydrophobic carbon pore walls. Consequently, although water molecules are not adsorbed on the pure microporous carbon at a low relative pressure, a predominant adsorption begins above the relative pressure at which the clusters are formed.[47−49] The active site mechanism of water molecules, that the surface functional group forms a hydrogen bond with a water molecule, inducing cluster formation, has been believed only with the adsorption measurement.[50] Iiyama and Kaneko have studied water adsorption with in situ X-ray diffraction and in situ X-ray scattering.[7,8,23] The obtained results do not contradict the active site mechanism. Also, they showed the cluster structure depending on the pore width; the water structure in the 0.7-nm pores is more ordered than that in the 1.1-nm pores due to a more intensive pseudocompression effect. In this case, the quasielectrolytic solution is formed in the micropores, and thereby ions of hydration anomaly and water molecular clusters of short range ordering should play an essential role in the NSN, which should be associated with the above pseudocompression effect. The pseudocompression effect gives rise to the Rb−O distance reduction and the coordination number change around a Br ion. In the 0.7-nm pore space of the greater pseudocompression effect, the Rb−O distance becomes shorter than that in the 1.1-nm space. Also the intensive confinement in the 0.7-nm pores deprives hydrated molecules of the Rb ion, transferring those water molecules to the vicinity of the Br ion. Thus, the coordination number around the Br ion is larger than that of the bulk solution irrespective of the invariant Br−O distance in the 0.7-nm pores. In the 1.1-nm pores there is room for the growth of water clusters that can provide large interaction energy with the pore wall. Hence, hydrated water molecules are deprived from both Rb and Br ions, leading to small coordination numbers for both Rb and Br ions. At the same time, the Rb−O distance becomes shorter with the pseudocompression effect. Thus, hydration structure anomaly sensitively depends on the pore width, which can be strongly supported by the following analysis.

TABLE 3: Structural Parameters Obtained by a Least-Squares Fit of Fourier-Filtered EXAFS of Rb K-Edge Spectra of NSNs with Eq 5[a]

sample	r_{Rb-O}/ nm	N_{Rb-O}	σ^2_{Rb-O}/ 10^{-5} nm^2
P20-NSN-1M	0.284(±0.002)	4.9(±0.2)	32.2(±0.5)
P20-NSN-0.1M	0.289(±0.001)	4.1(±0.1)	33.3(±0.2)
P5-NSN-1M	0.285(±0.001)	3.9(±0.1)	14.2(±0.3)
RbBr soln (1 M)	0.310(±0.002)	6.0[b]	42.6(±0.1)

sample	$C_{3,Rb-O}$/ 10^{-6} nm^3	$C_{4,Rb-O}$/ 10^{-8} nm^4	R_{Rb-O}/ %
P20-NSN-1M	2.0(±0.4)	3.9(±0.1)	7.4
P20-NSN-0.1M	2.1(±0.1)	5.9(±0.2)	5.5
P5-NSN-1M	3.2(±0.2)	−4.6(±0.1)	6.4
RbBr soln (1 M)	5.7(±0.5)	5.1(±0.2)	6.0

[a] The parameters are interatomic distance r, relative coordination number N, Debye−Waller factor σ, cumulant terms C_3 and C_4, and R-factor R. The first and second elements in the subscripts denote the central and scattering atoms, respectively. [b] Fixed parameter.

3.4. Hydration Structure Anomaly in Nanospaces from Cumulant Expansion Analysis. A cumulant expansion analysis of an EXAFS spectrum provides an accurate average structure because the coordination distance without cumulant analysis for the system including asymmetric potential structure provides a smaller value than the exact one.[51] The pore size effect described above should be more precisely analyzed and needs additional information on the local structure around ions in micropores, although a clear hydration anomaly due to the pseudocompression effect was shown.

Bunker reported the cumulant expansion method to analyze the EXAFS function.[52] The EXAFS formula shown in eq 3 can be written with cumulant terms as:[53]

$$\chi(k) = \frac{N|F(k)|e^{-2r/\lambda(k)}}{kr^2} \exp\left(-2\sigma^2k^2 + \frac{2}{3}C_4k^4\right) \sin\left(2kr + \phi(k) - \frac{4}{3}C_3k^3\right) \quad (5)$$

Here, C_n can be called the cumulant of nth order. This equation approximately neglects the higher cumulants and then shows the EXAFS function until the fourth-order cumulant. In the case of the EXAFS formula, the cumulant terms can be written as:

$$C_3 = \langle(\Delta r)^3\rangle$$

$$C_4 = \langle(\Delta r)^4\rangle - 3\sigma^4 \quad (6)$$

Here, Δr is a difference of coordination distance from an average one and $\langle ... \rangle$ is an average of each fluctuation term of the nth cumulant. Therefore, the curve fitting by with eq 5 can provide a precise structural model including thermal and static asymmetric effects. Tables 3 and 4 show the parameters obtained by the analysis with eq 5. All the R-factors around each Rb ion are smaller than those shown in Table 2, indicating that the cumulant expansion analysis is effective for the Rb ion. Accordingly, the structural parameters around a Rb ion in Table 3 are more reliable than those in Table 2. However, the literature values of the Rb−O distance and coordination number are not necessarily unique: 0.287−0.312 nm of the Rb−O distance and 4−12 of the coordination number are reported.[36−40] This is because the structure around a Rb ion cannot be sufficiently

TABLE 4: Structural Parameters Obtained by a Least-Squares Fit of Fourier-Filtered EXAFS of Br K-Edge Spectra of NSNs with Eq 5[a]

sample	r_{Br-O}/ nm	N_{Br-O}	σ^2_{Br-O}/ 10^{-5} nm^2
P20-NSN-1M	0.327(±0.001)	4.1(±0.1)	16.5(±0.4)
P20-NSN-0.1M			
P5-NSN-1M	0.318(±0.005)	9.1(±0.7)	30.5(±1.6)
RbBr soln (1 M)	0.314(±0.004)	6.0[b]	25.5(±3.8)

sample	$C_{3,Br-O}$/ 10^{-6} nm^3	$C_{4,Br-O}$/ 10^{-8} nm^4	R_{Br-O}/ %
P20-NSN-1M	0.8		5.6
P20-NSN-0.1M			
P5-NSN-1M	0.4		16.1
RbBr soln (1 M)	6.3		9.7

[a] The parameters are interatomic distance r, relative coordination number N, Debye−Waller factor σ, cumulant terms C_3 and C_4, and R-factor R. The first and second elements in the subscripts denote the central and scattering atoms, respectively. [b] Fixed parameter.

evaluated with XRD using Mo Kα radiation to carry out the electron radial distribution analysis. Here we fixed 6 as the coordination number in the cumulant expansion analysis for bulk aqueous solution. Thus we obtained the Rb−O distance for the bulk solution as 0.310 nm, being larger than that in Table 2. The Rb−O distance of NSNs is smaller than the 0.310 nm value for the bulk solution. All the coordination numbers of NSNs are smaller than 6. Hence, the results on the local structure around a Rb ion from the cumulant expansion analysis are almost similar to those shown above except for the coordination number of NSN of P5. The coordination number of NSN of P5 is smaller than those of NSNs of P20, being different from those in Table 2. The advanced analysis evidences clearly that the hydration structure around a Rb ion in the 0.7-nm pore is more compressed with lower coordination number than those in the 1.1-nm pore. Also the DW factor of P5-NSN-1M is the smallest, indicating the highly compressed state of NSN in the 0.7-nm pore .

The cumulant terms (C_3 and C_4) lead to detailed information on the hydration structure in addition to the average coordination structures. The C_3 values for NSNs are smaller than those of RbBr aqueous solution, suggesting the presence of the pseudocompression effect. Also, C_4 for only P5-NSN-1M is a negative value, indicating a remarkable pseudo-high-pressure effect that molecular assemblies confined in the nanospace behave as the condensed phase at low temperature. This negative C_4 for P5-NSN-1M supports the above conclusion, because the first perturbation term of C_4 is negative in the condensed phase at low temperature, leading to a negative total C_4 value.[54] The value of C_3 for P5-RbBr-1M is larger than that for NSNs in P20, reflecting an asymmetry dependence of the narrow slit shape. The pore potential is a function of the distance of a molecule from the pore wall; the potential profiles of the vertical and horizontal directions of slit-pores are completely different. The asymmetry of pore potential lead to a larger value of C_3 for P5-NSN-1M even if the compression effect by the nanospaces is great. Thus the cumulant terms express the pore-width dependence of the asymmetric nanoconfinement effect on the hydrated structure around a Rb ion. Accordingly, the hydrated water molecules around a Rb ion of NSNs should form more rigid structure than that of bulk aqueous solution. Thus the pseudocompression effect evidently decreases these parameters.

On the other hand, the cumulant expansion analysis of NSNs around a Br ion gives results different from those of the Rb ion, as shown in Table 4. The fitting with C_4 values did not converge with reasonable fitting parameters. Then the C_4 must be neglected in curve fitting with cumulant terms, because the error of C_4 in the analysis is generally larger than other parameters. In the analysis of NSNs around a Br ion, only the C_3 parameter was used for the cumulant expansion analysis. The asymmetric effects for this system are relatively negligible, because all C_3 values are quite small compared with those of Rb ions of NSNs and R-factors are not small irrespective of the additional cumulant terms. Thus the precise parameters could not be determined with cumulant expansion analysis for NSNs around a Br ion. According to the previous studies on the hydration structure of a Br ion in the bulk solution, water molecules must be weakly hydrated with a Br ion;[55,56] water molecules around an anion form a hydrogen bond associated structure and some parts of these hydrogen bonds are broken for an effective hydration around the Br ion.[57] Also the EXAFS of the K-edge Br spectrum includes the scattering wave depending on the double excitation of electronic states.[58,59] The peak at the nearest distance in the RSF can be influenced by the double excitation, if the concerned shell is constructed by light atoms. Consequently the large R-factor around a Br ion shown in Tables 2 and 4 should come from the complex electronic structures of a Br ion. Thus it is so difficult to analyze more fully the hydration structure around a Br ion owing to the double excitation effect that further analyses with other methods are needed to elucidate. However, we obtain the relative difference between P5 and P20 for the hydration structure around a Br ion irrespective of the large R-factor. That is, the larger coordination distance and the smaller coordination number of P20-NSN-1M than those in P5 suggest that the coordinated water molecules around a Br ion in P20 are transferred to form cluster-mediated ordered structures.

4. Conclusion

The hydration structure around a Rb ion of NSN is different from that of bulk solution. Rb−H_2O distances, hydration numbers, and DW factors of NSNs indicate the presence of highly compressed structures of partial dehydration in the hydrophobic micropores. As the slit width is an order of the molecular size, the above effect of the confinement of Rb ions depends sensitively on the pore width. In the 0.7-nm micropores, an intensive confinement effect induces highly compressed and distorted hydration structures compared with those in the 1.1-nm micropores. In the case of 1.1-nm micropores, less compressed and distorted hydration structures are observed and a portion of the hydrated water molecules are dissociated to form a stable ordered structure of water molecules in the 1.1-nm micropores.

On the contrary, the hydration structural changes around a Br ion due to the confinement by the 0.7- and 1.1-nm micropores are different from each other with relevance to the structure of the bulk solution. The distinct difference between Rb and Br ions must be studied in other nanoporous systems in the future. The confinement of "ionic solution" in the nanoscale space surrounded by the hydrophobic walls can provide a new chemistry that is associated with the principal concept in chemistry, although still this type of study is at an early stage.

Acknowledgment. This work has been performed under the approval of the Photon Factory Program Advisory Committee (Proposal No. 2002G242). Also this work was supported by Research Fellowships of the Japan Society for the Promotion of Science (JSPS) for Young Scientists and the nanocarbon project by the New Energy Development Organization (NEDO).

References and Notes

(1) Rouquerol, F.; Rouquerol, J.; Sing, K. S. W. *Adsorption by Powders & Porous Solids*; Academic Press: London, UK, 1999.
(2) Conway, B. E. *Electrochemical Supercapacitors*: *Scientific Fundamentals and Technological Application*; Kluwer Academic/Plenum Publishers: New York, 1999.
(3) Kaneko, K.; Shimizu, K.; Suzuki, T. *J. Chem. Phys.* **1992**, *98*, 8705.
(4) Kanoh, H.; Kaneko, K. *J. Phys. Chem.* **1995**, *99*, 5746.
(5) Kaneko, K. *Colloid Surf.* **1996**, *109*, 319.
(6) Kaneko, K. *Carbon* **2000**, *38*, 287.
(7) Iiyama, T.; Nishikawa, K.; Otowa, T.; Kaneko, K. *J. Phys. Chem.* **1995**, *99*, 10075.
(8) Iiyama, T.; Nishikawa, K.; Suzuki, T.; Kaneko, K. *Chem. Phys. Lett.* **1997**, *274*, 152.
(9) Ohkubo, T.; Iiyama, T.; Nishikawa, K.; Suzuki, T.; Kaneko, K. *J. Phys. Chem. B* **1999**, *103*, 1859.
(10) Ohkubo, T.; Iiyama. T.; Kaneko, K. *Chem. Phys. Lett.* **1999**, *312*, 191.
(11) Iiyama, T.; Nishikawa, K.; Suzuki, T.; Kaneko, K. *J. Phys. Chem. B* **1997**, *101*, 3037.
(12) Kaneko, K.; Fukuzaki, N.; Ozeki, S. *J. Chem. Phys.* **1987**, *87*, 776.
(13) Aoshima, M.; Suzuki, T.; Kaneko, K. *Chem. Phys. Lett.* **1999**, *310*, 1.
(14) Miyahara, M.; Gubbins, K. E. *J. Chem. Phys.* **1997**, *106*, 2865.
(15) Watanabe, A.; Iiyama. T.; Kaneko, K. *Chem. Phys. Lett.* **1999**, *305*, 71.
(16) Kaneko, K.; Watanabe, A.; Iiyama. T.; Radhakrishan, R.; Gubbins, K. E. *J. Phys. Chem. B* **1999**, *103*, 7061.
(17) Radhakrishnan, R.; Gubbins, K. E.; Watanabe, A.; Kaneko, K. *J. Chem. Phys.* **1999**, *111*, 9058.
(18) Frank, H. S.; Wen, W. Y. *Discuss. Faraday Soc.* **1957**, *24*, 133.
(19) Hribar, B.; Southall, N. T.; Vlachy, V.; Dill, K. A. *J. Am. Chem. Soc.* **2002**, *124*, 12302.
(20) Ferlat, G.; San Miguel, A.; Jal, J. F.; Soetens, J. C.; Bopp, Ph. A.; Daniel, I.; Guillot, S.; Hazemann, J. L.; Argoud, R. *Phys. Rev. B* **2001**, *63*, 134202/1.
(21) Ferlat, G.; San Miguel, A.; Jal, J. F.; Soetens, J. C.; Bopp, Ph. A.; Hazemann, J. L.; Testemale, D.; Daniel, I. *J. Mol. Liq.* **2002**, *127*, 127.
(22) Fulton, J. L.; Pfund, D. M.; Wallen, S. L.; Newville, M.; Stern, E. A.; Ma, Y. *J. Chem. Phys.* **1996**, *105*, 2161.
(23) Iiyama, T.; Ruike, M.; Kaneko, K. *Chem. Phys. Lett.* **2001**, *331*, 359.
(24) Kimura, T.; Kanoh, H.; Kaneko, K. *J. Phys. Chem.* In preparation.
(25) Ohkubo, T.; Konishi, T.; Hattori, Y.; Kanoh, H.; Fujikawa, T.; Kaneko. K. *J. Am. Chem. Soc.* **2002**, *124*, 11860.
(26) Kaneko, K.; Ishii, C.; Ruike, M.; Kuwabara, H. *Carbon* **1992**, *30*, 1075l.
(27) Suzuki, T.; Kasuh, T.; Kaneko, K. *Chem. Phys. Lett.* **1992**, *191*, 569.
(28) Ishii, C.; Suzuki, T.; Shindo, N.; Kaneko, K. *J. Porous Mater.* **1997**, *4*, 181.
(29) Kaneko, K.; Ishii, C.; Kanoh, H.; Hanzawa, Y.; Setoyama, N.; Suzuki, T. *Adv. Colloid Interface Sci.* **1998**, *76*−*77*, 295.
(30) Merraoui, M. E.; Aoshima, M.; Kaneko, K. *Langmuir* **2000**, *16*, 4300.
(31) Fox, B. S.; Petru Balaj, O.; Balteanu, I.; Beyer, M. K.; Bondybey, V. E.; *Chem. Eur. J.* **2002**, *8*, 5534.
(32) Kaneko, K.; Ishii, C. *Colloid Surf.* **1992**, *67*, 203.
(33) Setoyama, N.; Suzuki, T.; Kaneko, K. *Carbon* **1998**, *36*, 1459.
(34) Teo, B. K. *EXAFS: Basic Principles and Data Analysis*; Springer-Verlag: Heidelberg, Germany, 1986.
(35) Ankudinov, A. L.; Ravel, B.; Rehr. J. J.; Conradson, S. D. *Phys. Rev. B* **1998**, *58*, 7565.
(36) Bertagnolli, H.; Frtel, T. S.; Hoffmann, M.; Frahm, R. *Ber. Bunsen-Ges. Phys. Chem.* **1991**, *95*, 704.
(37) Vogrin, B. F. J.; Knapp, P. S.; Flint, W. L.; Anton, A.; Highberger, G.; Malinowski, E. R. *J. Chem. Phys.* **1971**, *54*, 178.
(38) Hinton, J. F.; Amis, E. S. *Chem. Rev.* **1971**, *71*, 629.
(39) Shannon, R. D. *Acta Crystallogr. A* **1976**, *32*, 751.
(40) Jia, Y. Q. *Solid State Chem.* **1991**, *95*, 184.
(41) Lee, P. A.; Citrin, P. H.; Eisenberger, P.; Kincaid, B. M. *Rev. Mod. Phys.* **1981**, *53*, 769.
(42) Ludwig, K. F., Jr.; Warburton, W. K.; Fontaine, A. *J. Chem. Phys.* **1987**, *87*, 620.
(43) Rao, R. V. G.; Das, R. *Phys. Status Solidi* **1988**, *110*, 347.
(44) D'Angelo, P.; Nola, A. D.; Filipponi, A.; Pavel, N. V.; Roccatano, D. *J. Chem. Phys.* **1994**, *100*, 985.
(45) Ramos, S.; Barnes, A. C.; Neilson, G. W.; Thiaudiere, D.; Lequien, S. *J. Phys.*: *Condens. Matter* **1999**, *11*, A203.
(46) http://ixs.csrri.iit.edu/ (IXS Standards and Criteria Committee).
(47) Kaneko, K.; Hanzawa, Y.; Iiyama, T.; Kanda, T.; Suzuki, T. *Adsorption* **1999**, *5*, 7.
(48) Brennan, J. K.; Thomson, K. T.; Gubbins, K. E. *Langmuir* **2002**, *18*, 5438.
(49) Ohba, T.; Kaneko, K. In preparation.
(50) Mowla, D.; Do, D. D.; Kaneko, K. *Chem. Phys. Carbon* **2003**, *28*, 229.
(51) Eisenberger, E.; Brown, G. S. *Solid State Commun.* **1979**, *29*, 481.
(52) Bunker, G. *Nucl. Instrum. Methods Phys. Res.* **1983**, *207*, 1488.
(53) Sakane, H.; Miyanaga, T.; Watanabe, I.; Matsubayashi, N.; Ikeda, S.; Yokoyama. Y. *Jpn. J. Appl. Phys.* **1993**, *32*, 4641.
(54) Yokoyama, T. *Phys. Rev. B* **1998**, *57*, 3423.
(55) Tanida, H.; Sakane, H.; Watanabe, I. *J. Chem. Soc., Dalton Trans.* **1994**, *15*, 2321.
(56) Tanida, H.; Watanabe, I. *Bull. Chem. Soc. Jpn.* **2000**, *73*, 2747.
(57) Ohtaki, H.; Radnai, T. *Chem. Rev.* **1993**, *93*, 1157.
(58) Li, G.; Bridges, F.; Brown, G. S. *Phys. Rev. Lett.* **1992**, *68*, 1609.
(59) D'Angelo, P.; Di Cicco, A.; Filipponi, A.; Pavel, N. V. *Phys. Rev. A* **1993**, *47*, 2055.